Transient Modeling of a Multi-Evaporator Air Conditioning System and Control Method Investigation

Hongtao Qiao, Laeun Kwon, Vikrant Aute, Reinhard Radermacher*
4164E Glenn Martin Hall, University of Maryland, College Park, MD, USA
**vikrant@umd.edu*

Abstract: In this paper, a transient mathematical model for a multi-split variable refrigerant flow (VRF) system having six indoor units is presented. The compressor is modeled using curve-fitted equations based on the performance map. The moving boundary method (MBM) is chosen to simulate the indoor and outdoor coils. Electronic expansion valves (EEVs) are modeled via empirical correlations. The conditioned rooms are emulated as lumped-parameter control volumes. With the aid of this transient system model, a control strategy is proposed. The compressor frequency is used to regulate the saturated suction temperature. EEV openings are used to control the superheat degree of the indoor coils. Room temperatures are regulated by hysteresis on-off control. Controllability test is carried out to demonstrate that the proposed control strategy is adequate to achieve individual zone control.

Key Words: transient modeling, control, multi-evaporator, air-conditioning

1 INTRODUCTION

Multi-split VRF systems are increasingly some gaining popularity over traditional air conditioning systems due to higher energy saving potential and better indoor thermal comfort as well as the ability of controlling individual zones. A typical VRF air conditioning system has a single outdoor unit and multiple indoor units, as shown in Figure 1. The outdoor unit incorporates a variable speed compressor, an accumulator and a condenser-fan coil, whereas each indoor unit encompasses an EEV (note: in some cases, EEVs are located in the condensing unit close to the compressor), an evaporator coil and an air circulating blower. Such a system exhibits much more complicated dynamics compared to the conventional systems with single evaporator because the operation in one zone may influence the units in other zones since all the evaporators are simultaneously served by one outdoor unit (Choi and Kim, 2003; Shah *et al*., 2003).

Over the past decade, both experimental and numerical studies have been extensively reported to explore the operating characteristics and control strategies of VRF systems. Park *et al*. (2001) analyzed the performance of a multi-type air conditioner with dual evaporators and pointed out the major control parameter of the system is the EEV opening. Choi and Kim (2003) conducted a series of experimental studies to scrutinize the capacity modulating characteristics of a VRF system with two indoor units by varying indoor load, EEV opening and compressor speed. It was concluded that VRF systems exhibit strong coupling effects between different indoor units and thus simultaneous control of compressor speed and EEV opening is required. Shah *et al*. (2004) presented a generalized dynamic modeling approach for multi-evaporator air-conditioning cycles. A strong cross coupling effect between different evaporators was observed in the simulation studies. Chen *et al*. (2005) developed a simplified lumped-parameter transient thermodynamic model for a triple-evaporator air conditioning system and proposed a novel control strategy that was embodied with a self-tuning fuzzy control algorithm. Chiou *et al*. (2009) experimentally revealed that the fuzzy control method can be effectively applied in VRF systems to improve energy efficiency and achieve a steady temperature regulation for the conditioned zones. Zhang and Zhang (2011) presented a validated dynamic model of a multi-indoor unit air conditioning system with a rapid cycling scroll compressor. Shao *et al*. (2012) developed a dynamic simulation model with the framework of two-phase fluid network to investigate the transient characteristics of

multi-unit air conditioners. The state-space forms are used to model the system and components, and the component models are embedded in the fluid network model, which makes it possible to update the system model and components models independently. Xu *et al*. (2013) proposed a novel capacity control algorithm for VRF systems which imitated the on/off control of a single evaporator air conditioning system. Zhu *et al*. (2013) developed generic simulation models based on TRNSYS to analyze the performance of VRF systems. With the aid of the developed models, system responses subject to the variations in the indoor and outdoor air temperatures, and EEV opening were inspected. No control strategy was reported. Elliott and Rasmussen (2013) introduced a decentralized control architecture for multiple evaporator cooling systems in which the compressor speed is used to regulate the suction pressure while the EEV opening and indoor coil fan speed are used to control the evaporator superheat and cooling rate set point.

Based on the above literature review, it can be concluded that although there are extensive studies on the performance evaluation and control methods of VRF systems, not many investigations have been focused on the transient modeling of such systems. The aim of this paper is to explore the dynamic behavior of a VRF heat pump system with six indoor units in the cooling mode from a numerical simulation perspective. First-principles models are developed for each component and all the models are linked together in a systematic manner to analyze the transient operating characteristics of the system. A control strategy whose intention is to maintain the desired indoor air temperatures is proposed. Case studies are carried out to demonstrate the capability of the developed models and the feasibility of the proposed control strategy.

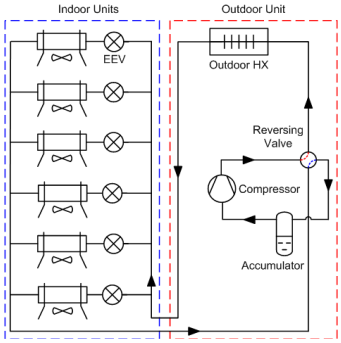

Figure 1: Schematic of a VRF system

2 MODEL DEVELOPMENT

2.1 Compressor model

In the transient simulation, the compressor is often regarded as a quasi-steady state component because the timescales associated with the variation of the compressor mass flow rate are very small compared to the timescales associated with heat exchangers and charge distribution. As a consequence, a full-scale physics-based compressor model that captures the detailed transients during the compression process is not necessary especially considering the associated computation cost (Winkler, 2009).

In the studied system, a variable-speed high-side shell scroll compressor is used, which means that the motor is cooled by the compressed high-pressure discharge refrigerant. The performance map, provided by the compressor manufacturer, is usually tabulated over a specific range of saturated discharge and suction temperatures and does not have a good accuracy when extrapolated beyond those temperature ranges. In light of this, it is wise to convert the map into curve-fitted equations to avoid potential pitfalls during the simulations.

The volumetric efficiency is a function of the suction pressure, discharge pressure and compressor frequency. It can be calculated by

$$\eta_v = c_0 + c_1\varphi + c_2\varphi^2 + c_3\varphi^3 + c_4\left(p_{dis} - p_{suc}\right)\left(1 + c_5 p_{suc}\right) \tag{1}$$

where

$$\begin{aligned}
\varphi &= \frac{p_{dis}}{p_{suc}} \\
c_0 &= a_1 + a_2\phi + a_3\phi^2 \\
c_1 &= a_4 + a_5\phi + a_6\phi^2 \\
c_2 &= a_7 + a_8\phi + a_9\phi^2 \\
c_3 &= a_{10} + a_{11}\phi + a_{12}\phi^2 \\
c_4 &= a_{13} + a_{14}\phi + a_{15}\phi^2 \\
c_5 &= a_{16} + a_{17}\phi + a_{18}\phi^2 \\
\phi &= \frac{f}{f_{nom}}
\end{aligned} \tag{2}$$

The power consumed by the compressor is determined by

$$\dot{W}_{comp} = z_1 p_{suc}\dot{V}_{suc}\left(\varphi^{z_2} - 1\right) + z_3 \tag{3}$$

where

$$\begin{aligned}
z_1 &= b_1 + b_2\phi + b_3\phi^2 \\
z_1 &= b_4 + b_5\phi + b_6\phi^2 \\
z_3 &= b_7 + b_8\phi + b_9\phi^2
\end{aligned} \tag{4}$$

The mass flow rate delivered by the compressor is determined by

$$\dot{m}_{comp} = \eta_v f \rho_{suc} V_{disp} \tag{5}$$

The enthalpy of the discharged refrigerant is calculated by

$$h_{dis} = \frac{\left(1-\xi\right)\dot{W}_{comp}}{\dot{m}_{comp}} + h_{suc} \tag{6}$$

where ξ is the fraction of the compressor power dissipated to the ambient.

2.2 Expansion device model

The mass flow rate through the EEV is determined by the flow coefficient, the flow area, the inlet density and the pressure difference across the valve

$$\dot{m}_{\exp} = C_v A\sqrt{\rho_{in}\Delta p} \tag{7}$$

The combined value of the product $C_v A$ can be readily obtained by regression based on the experimental data

$$C_v A = \lambda_0 + \lambda_1 \vartheta + \lambda_2 \vartheta^2 \tag{8}$$

where ϑ is the percentage of valve opening determined by the PI (proportional-integral) controller based on the error between the measured superheat and the set point, $e_{sh}(t)$

$$\vartheta(t) = K_p e_{sh}(t) + K_i \int_0^t e_{sh}(\tau)\, d\tau \tag{9}$$

2.3 Accumulator model

The accumulator is modeled as a lumped control volume with an inlet and an outlet (Figure 2) by adopting the following simplifications:

(1) Ideal phase separation is assumed.
(2) Vapor and liquid in the accumulator are in thermodynamic equilibrium and thus there is no heat exchange between them.
(3) Pressure drop inside the accumulator is negligible.
(4) Accumulator is assumed to be adiabatic.

The governing equations for the accumulator can be described as follows

$$V_{acc} \frac{d\overline{\rho}_{acc}}{dt} = \dot{m}_{in} - \dot{m}_{out} \tag{10}$$

$$V_{acc} \left(\overline{\rho}_{acc} \frac{d\overline{h}_{acc}}{dt} - \frac{dp_{acc}}{dt} \right) = \dot{m}_{in} \left(h_{in} - \overline{h}_{acc} \right) - \dot{m}_{out} \left(h_{out} - \overline{h}_{acc} \right) \tag{11}$$

The leaving enthalpy is dependent upon the state of the refrigerant in the accumulator. There are two cases which need to be taken into account: 1) the refrigerant state is two-phase ($h_f < \overline{h}_{acc} < h_g$) and 2) the refrigerant state is single-phase ($\overline{h}_{acc} <= h_f$ or $\overline{h}_{acc} >= h_g$).

Case 1: the enthalpy of the outlet stream is determined as

$$h_{out} = \begin{cases} h_f & \text{if } H_{liq} > H_{out} + d_{out} \\ h_g - \left(\dfrac{H_{liq} - H_{out}}{d_{out}} \right) \left(h_g - h_f \right) & \text{if } H_{out} + d_{out} \geq H_{liq} \geq H_{out} \\ h_g & \text{if } H_{liq} < H_{out} \end{cases} \tag{12}$$

where the liquid height is determined as

$$H_{liq} = \frac{\overline{\rho}_{acc} - \rho_g}{\rho_f - \rho_g} H_{acc} \tag{13}$$

Case 2: the enthalpy of the outlet stream should be equal to the mean enthalpy of the refrigerant in the accumulator

$$h_{out} = \overline{h}_{acc} \tag{14}$$

The outlet mass flow rate can be calculated by

$$\dot{m}_{out} = \frac{\sqrt{(p_{acc} - p_{out})}}{f_{acc}} \tag{15}$$

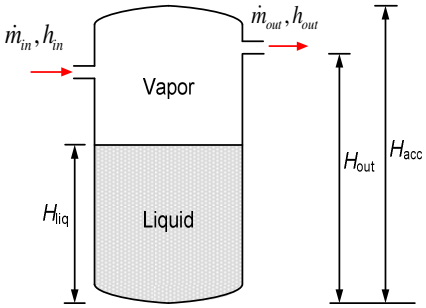

Figure 2: Schematic of an accumulator

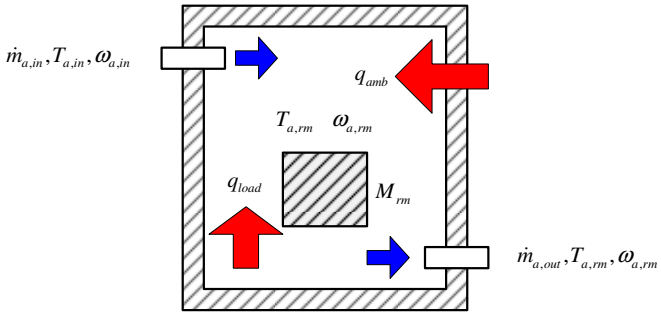

Figure 3: Lumped-parameter room model

2.4 Room model

The conditioned rooms are emulated as lumped-parameter control volumes, as shown in Figure 3. Assuming that the objects inside the room are in thermal equilibrium with the indoor air, the governing equations that calculate the time-derivative of air temperature and humidity ratio can be easily formulated as

$$\left(M_{rm}c_{p,rm} + V_{rm}\rho_{air,rm}c_{p,air}\right)\frac{dT_{a,rm}}{dt} = \dot{m}_{a,in}h_{a,in} - \dot{m}_{a,out}h_{a,rm} + q_{amb} + q_{load} \tag{16}$$

$$\rho_{air,rm}V_{rm}\frac{d\omega_{a,rm}}{dt} = \dot{m}_{a,in}\omega_{a,in} - \dot{m}_{a,out}\omega_{a,rm} \tag{17}$$

Please note that $h_{a,in}$ and $\omega_{a,in}$ should be the state of air leaving the indoor coil, $h_{a,out}$ and $\omega_{a,out}$ should be the state of air entering the indoor coil.

2.5 Heat exchanger model

The heat exchangers exert the most influence on the transient thermal performance of vapor compression systems, and it is essential to derive an adequate modeling representation which can describe the main heat transfer and flow phenomena in the condenser and evaporator.

Although distributed models render the most accurate predictions, they are not generally well suited for control design where low order models are more favorable. A class of low order models can be categorized as moving boundary models which are superior to distributed models for control purposes. They are characterized by dividing the heat exchanger into control volumes each of which exactly compasses a particular fluid phase (superheated vapor, two-phase flow, subcooled liquid). The control volumes are separated by a moving interface where the refrigerant phase transition occurs. In contrast to the distributed models, the number of control volumes in moving boundary models may vary depending on the

number of available phases currently present within the heat exchanger. Therefore, a heat exchanger may own three control volumes at most and one control volume at least at a time. The objective of these models is to capture the thermodynamic behavior inside these control volumes and the time-varying positions of phase boundaries.

Moving boundary method is used to analyze the heat exchangers. For the sake of brevity, we only show the formulations for the condenser model in the paper, as shown in Figure 4. The formulations of the evaporator model can be derived similarly.

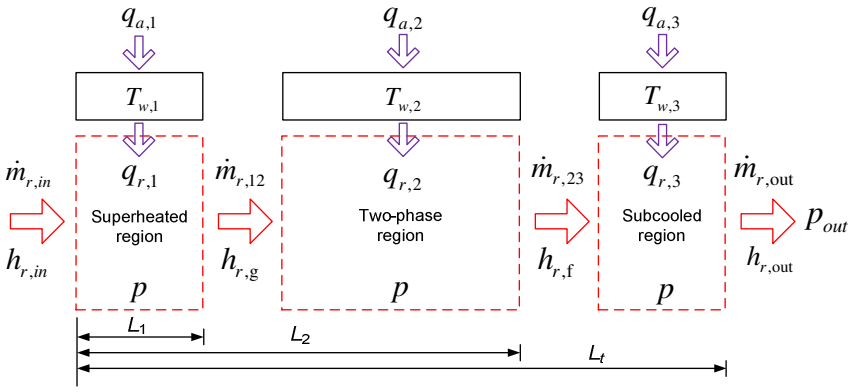

Figure 4: Moving boundary condenser model

Superheated region

$$A_c L_1 \frac{d\overline{\rho}_1}{dt} + A_c\left(\overline{\rho}_1 - \rho_g\right)\frac{dL_1}{dt} = \dot{m}_{r,in} - \dot{m}_{r,12} \tag{18}$$

$$A_c L_1\left(\overline{\rho}_1 \frac{d\overline{h}_1}{dt} + \overline{h}_1 \frac{d\overline{\rho}_1}{dt} - \frac{dp}{dt}\right) + A_c\left(\overline{\rho}_1\overline{h}_1 - \rho_g h_g\right)\frac{dL_1}{dt} = \dot{m}_{r,in}h_{r,in} - \dot{m}_{r,12}h_g + q_{r,1} \tag{19}$$

$$\frac{dT_{w,1}}{dt} = \frac{q_{a,1} - q_{r,1}}{c_{p,w}\rho_w A_{c,w} L_1} + \frac{T_{w,2} - T_{w,1}}{L_2}\frac{dL_1}{dt} \tag{20}$$

Two-phase region

$$A_c\left(L_2 - L_1\right)\left[\left(1-\overline{\gamma}\right)\frac{d\rho_f}{dp} + \overline{\gamma}\frac{d\rho_g}{dp}\right]\frac{dp}{dt} + A_c\left(\rho_g - \rho_f\right)\overline{\gamma}\frac{dL_2}{dt} - A_c\left(\rho_g - \rho_f\right)\left(\overline{\gamma}-1\right)\frac{dL_1}{dt} + A_c\left(\rho_g - \rho_f\right)\left(L_2 - L_1\right)\frac{d\overline{\gamma}}{dt} = \dot{m}_{r,12} - \dot{m}_{r,23} \tag{21}$$

$$A_c\left(L_2 - L_1\right)\left[\left(1-\overline{\gamma}\right)\frac{d\left(\rho_f h_f\right)}{dp} + \overline{\gamma}\frac{d\left(\rho_g h_g\right)}{dp}\right]\frac{dp}{dt} + A_c\left(\rho_g h_g - \rho_f h_f\right)\overline{\gamma}\frac{dL_2}{dt} - A_c\left(\rho_g h_g - \rho_f h_f\right)\left(\overline{\gamma}-1\right)\frac{dL_1}{dt} + A_c\left(\rho_g h_g - \rho_f h_f\right)\left(L_2 - L_1\right)\frac{d\overline{\gamma}}{dt} = \dot{m}_{r,12}h_f - \dot{m}_{r,23}h_g + q_{r,2} \tag{22}$$

$$\frac{dT_{w,2}}{dt}=\frac{q_{a,2}-q_{r,2}}{c_{p,w}A_{c,w}\rho_w\left(L_2-L_1\right)}+\frac{T_{w,2}-T_{w,1}}{L_2}\frac{dL_1}{dt}+\frac{T_{w,3}-T_{w,2}}{L_t-L_1}\frac{dL_2}{dt} \tag{23}$$

Subcooled region

$$A_c\left(L_t-L_2\right)\frac{d\bar{\rho}_3}{dt}-A_c\left(\bar{\rho}_3-\rho_f\right)\frac{dL_2}{dt}=\dot{m}_{r,23}-\dot{m}_{r,out} \tag{24}$$

$$A_c\left(L_t-L_2\right)\left(\bar{\rho}_3\frac{d\bar{h}_3}{dt}+\bar{h}_3\frac{d\bar{\rho}_3}{dt}-\frac{dp}{dt}\right)-A_c\left(\bar{\rho}_3\bar{h}_3-\rho_f h_f\right)\frac{dL_2}{dt} \tag{25}$$
$$=\dot{m}_{r,23}h_f-\dot{m}_{r,out}h_{r,out}+q_{r,3}$$

$$\frac{dT_{w,3}}{dt}=\frac{q_{a,3}-q_{r,3}}{c_{p,w}A_{c,w}\rho_w\left(L_t-L_2\right)}+\frac{T_{w,3}-T_{w,2}}{L_t-L_1}\frac{dL_2}{dt} \tag{26}$$

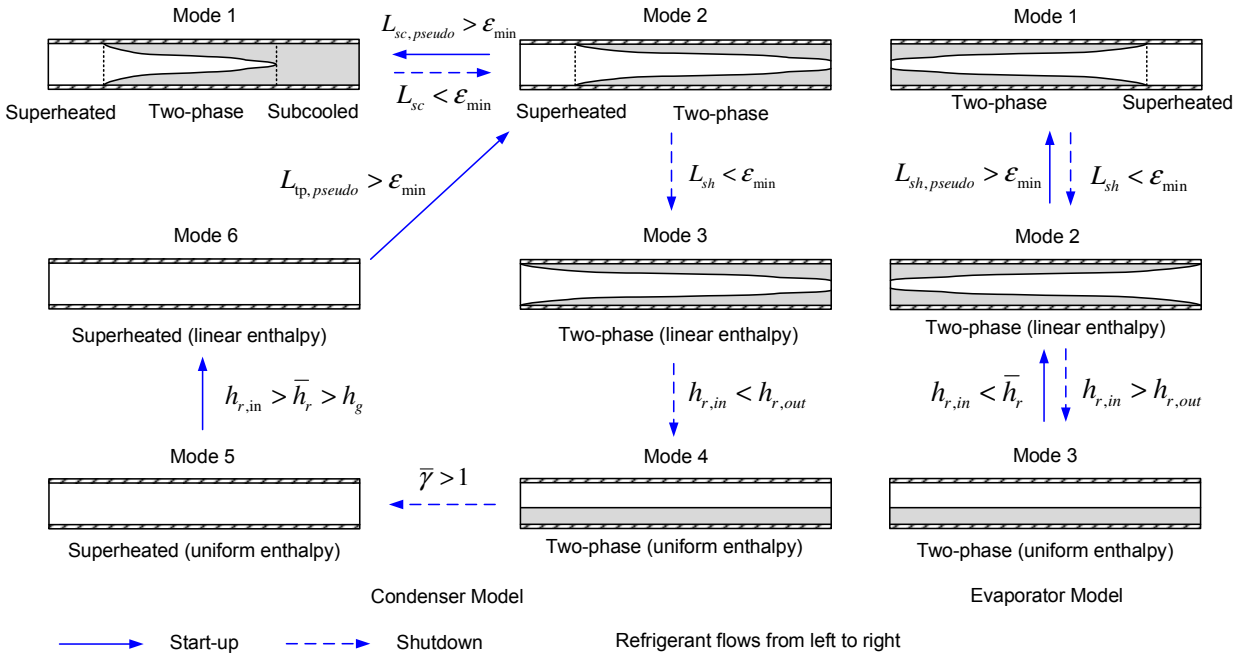

Figure 5: Different modes of moving boundary heat exchanger models

Switching criteria

As stated previously, the number of available fluid phases in the heat exchanger may vary under large disturbances and fluid phases can disappear or reappear. Therefore, moving boundary models equipped with switching schemes are needed to ensure smooth transition between different model representations when fluid phases form or disappear. Although recent research efforts for moving boundary method have been focused on tackling drastic transients experienced by heat exchangers operating under cycling conditions (Li and Alleyne, 2010), these types of models are inherently not as robust as distribute models because of the resulting potential numerical failures associated with model transition.

In light of this, the paper proposes a consistent, comprehensive and robust switching approach to handle transitions between different model representations given the fact that the switching methods presented in the literature have flaws and may cause serious

instabilities when it comes to the simulation of cycling transients. All the modes experienced by heat exchangers under cycling conditions and the switching criteria between different modes are shown in Figure 5. The minimum threshold $\varepsilon_{\min}$ can be adjusted based on the application. The pseudo length is determined based on the mass conservation as follows:

$$L_{pseudo} = \frac{\overline{\rho}_{new\,zone\&adjacent\,zone} - \overline{\rho}_{adjacent\,zone}}{\overline{\rho}_{new\,zone} - \overline{\rho}_{adjacent\,zone}} L_{adjacent\,zone} \tag{27}$$

3 DEVELOPMENT OF CONTROL STRATEGY

VRF systems exhibit unique operating characteristics compared to the conventional air-conditioners. Their control strategies are also much more complicated than those of the conventional systems. Since the control strategies of VRF systems are often regarded as confidential, they are not commonly discussed in open literature. This paper tries to put forward a feasible control strategy for the studied system to maintain the indoor air temperatures during the operation in summer. This strategy can be summarized as follows:

(1) If $T_{a,rm} > T_{a,set} + \Delta T$, EEV is open to control the evaporator superheat and indoor coil fan is turned on.
(2) If $T_{a,rm} < T_{a,set} - \Delta T$, EEV is closed and indoor coil fan is turned off.
(3) If $T_{a,set} - \Delta T < T_{a,rm} < T_{a,set} + \Delta T$, the status of EEV and indoor coil fan keeps unchanged.
(4) The compressor frequency is used to regulate the saturated suction temperature.
(5) The compressor is turned off when all the indoor units are switched off.
(6) EEV openings and compressor frequency are controlled by PI controller.

4 IMPLEMENTATION

The proposed transient models are implemented using the Modelica modeling language and the Dymola 7.4 simulation environment. All the refrigerant properties are evaluated using the in-house curve-fitted property routines developed based upon the REFPROP 9.0 database (Lemmon *et al.*, 2010). The curve-fitting property routines can substantially speed up the computation without significant loss of accuracy. In this study, empirical correlations were used to calculate the heat transfer coefficients on both refrigerant and air side in the models for heat exchangers. The correlations proposed by Wang *et al.* (1999 & 2000) are chosen to calculate the heat transfer for louver fin geometry since the louver fin-and-tube heat exchangers are used in the studied system. Zivi (1964) correlation is selected to calculate the two-phase void fraction because of its simplicity. Gnielinski correlation (1976) is chosen to calculate the heat transfer coefficient for single-phase flows. Dobson-Chato correlation (1998) and Gungor-Winterton correlation (1987) are used to calculate the heat transfer coefficients for two-phase flows.

5 CASE STUDY

The studied system in the paper has six indoor units with different capacities. In order to verify the validity of the developed models and the proposed control strategy, a pull-down transient simulation is carried out. Before the simulation, all the indoor air temperatures are at 35°C, the same as the ambient temperature. When the system starts, the indoor air temperatures will start to drop and will be maintained within the desired range. The system operates for 10,000 seconds. The operating conditions of the studied system are listed in Table 1. The simulation results are shown in Figure 6 and 7.

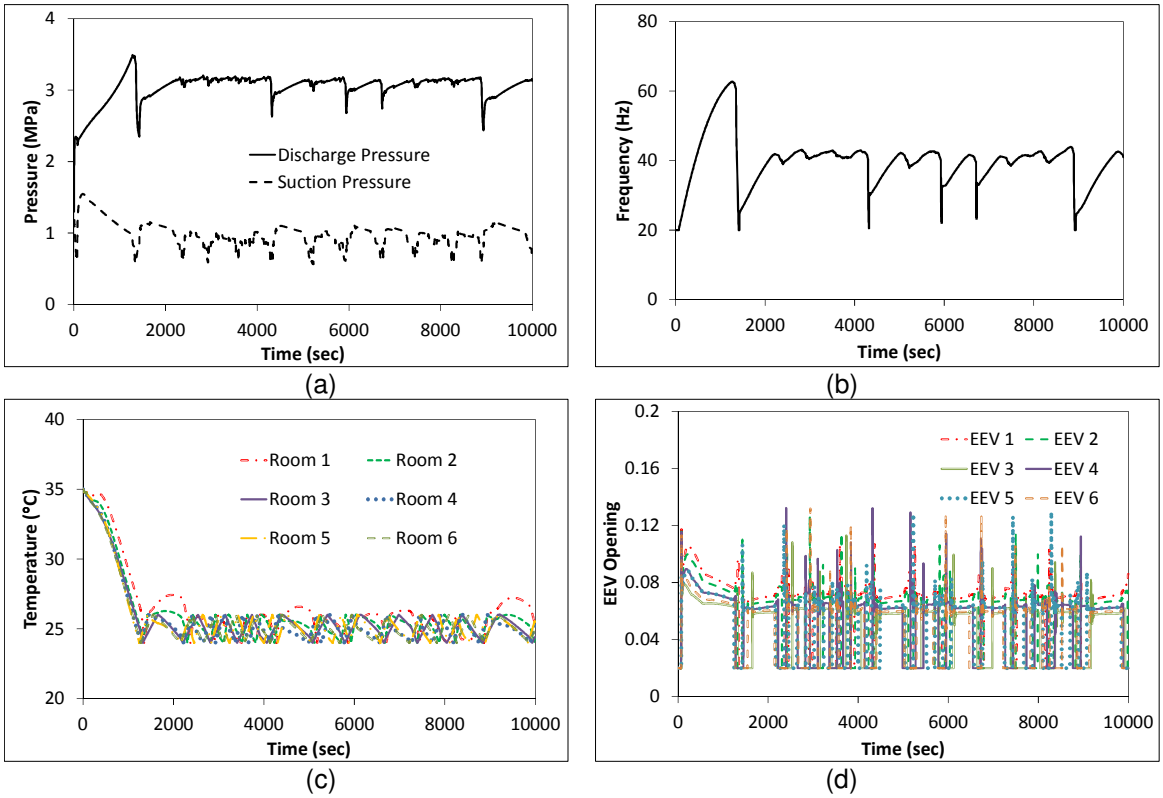

Figure 6: (a) pressure vs. time, (b) compressor frequency vs. time, (c) room air temperature vs. time, (d) EEV opening vs. time

Figure 6a shows the variations in suction pressure and discharge pressure. It can be observed that the suction pressure exhibits obvious fluctuations, which is caused by the variations in EEV openings. At the very beginning of the pull-down process, the suction pressure shows a sudden decrease for two reasons, i.e. 1) the compressor starts to draw a significant amount of refrigerant out of the accumulator and 2) EEVs are initially closed when the system starts up. After a short period, the suction pressure starts to rise because EEV openings increase. After 200 seconds, the suction pressure starts to drop again because the indoor air is cooling down. Compared to the suction pressure, the discharge pressure undergoes much more benign variations except that it increases continuously during the pull-down period. The abrupt change in the discharge pressure thereafter is due to the sudden variations in the compressor frequency seen in Figure 6b. Figure 6c illustrates the variations in indoor air temperature for each room. Figure 6d represents the variations in EEV openings. All the EEVs can quickly respond to the required cooling capacity.

Figure 7a shows the capacity variations in each indoor unit. These six indoor units deliver different capacities that increase with the rise in the compressor frequency. Figure 7b demonstrates the variations in the suction temperature and discharge temperature as well as the compressor power. The suction temperature oscillates around 15°C, while the discharge temperature oscillates around 90°C. The compressor power is proportional to the variations of the compressor frequency. Figure 7c shows the variations in refrigerant mass flow through all the indoor units. Figure 7d illustrates the refrigerant mass distribution within the various components during the operation. Over 80 percent of refrigerant mass is located in the outdoor coil that serves as the condenser. The remainder is distributed within the accumulator and indoor coils.

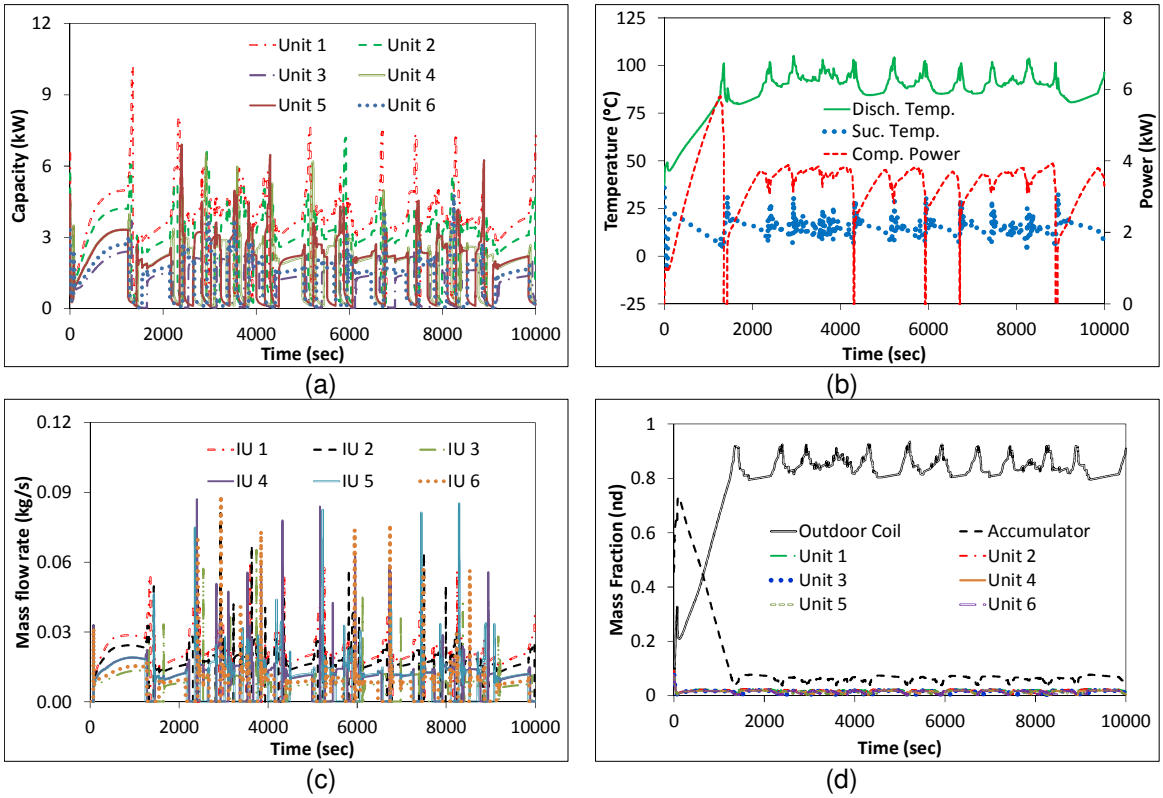

Figure 7: (a) indoor unit capacity vs. time, (b) suction temperature, discharge temperature & compressor power vs. time, (c) refrigerant mass flow rate vs. time, (d) refrigerant mass distribution vs. time

Table 1: Operating conditions of the VRF system

Parameter	Value
Outdoor ambient temperature	35°C
Thermal load of each room	
Room 1	3.6 kW
Room 2	2.7 kW
Room 3	0.9 kW
Room 4	1.7 kW
Room 5	1.6 kW
Room 6	1.1 kW
Room air temperature setting	25±1°C
Compressor frequency	0 ~ 120 Hz

6 CONCLUSIONS

VRF systems exhibit more complicated dynamics compared to conventional single-evaporator systems. In this paper, a transient model for a VRF system with six indoor units is developed. Heat exchangers are modeled with the moving boundary method that is equipped with a comprehensive and robust switching scheme. Other components are analyzed using a lumped-parameter method. Considering unique operating characteristics of VRF systems, a control strategy that maintains the indoor air temperatures at set values is proposed. The compressor frequency is used to regulate the saturated suction temperature. EEV openings are used to control the superheat degree of the evaporator coils. Room temperatures are regulated by hysteresis on-off control. Controllability test showed that the proposed control strategy is feasible to achieve individual zone control.

7 NOMENCLATURES

Abbreviations

A	area [m^2]
a_1-a_{18}	regression constants [-]
b_1-b_9	regression constants [-]
c_p	specific heat [J/kg-K]
C_v	flow coefficient [-]
d	diameter [m]
e_{sh}	error between the measured superheat and the set point [K]
f	frequency [Hz] or pressure loss coefficient [-]
h	enthalpy [kJ/kg]
H	height [m]
K_i	Integral gain [-]
K_p	proportional gain [-]
L	length [m]
$\dot{m}$	mass flow rate [kg/s]
M	mass [kg]
p	pressure [Pa]
q	heat transfer rate [W]
T	temperature [K]
V	volume [m^3]
$\dot{V}$	volumetric flow rate [m^3/s]
$\dot{W}$	power [W]
Δ	difference

Greek Symbols

ε	minimum length [m]
φ	pressure ratio [-]
ϕ	normalized frequency [-]
γ	void fraction [-]
ξ	fraction of the compressor power dissipated to the ambient [-]
ρ	density [kg/m^3]
λ_0 - λ_2	regression constant [-]
ω	humidity ratio [kg H_2O/kg dry air]
ϑ	EEV opening fraction [-]
η	efficiency [-]
τ	integral variable

Subscripts

a	moist air	min	minimum
acc	accumulator	new zone	new zone
adjacent zone	adjacent zone	nom	nominal
amb	ambient	out	outlet
c	cross section	pseudo	pseudo
comp	compressor	r	refrigerant
dis	discharge	rm	room
disp	displacement	set	set point
exp	expansion device	sh	superheat
f	saturated liquid	suc	suction
g	saturated vapor	t	tube
in	inlet	tp	two-phase
liq	liquid	v	volumetric
load	load	w	tube wall

8 REFERENCES

1. Chen, W., Zhou, X., Deng, S., 2005. Development of control method and dynamic model for multi-evaporator air conditions (MEAC). Energy Conversion and Management 46, 451-465.
2. Chiou, C.B., Chiou, C.H., Chu, C.M., Lin, S.L., 2009. The application of fuzzy control on energy saving for multi-unit room air-conditioners. Applied Thermal Engineering 29, 310-316.
3. Choi, J.M. and Kim, Y.C., 2003. Capacity modulation of an inverter-driven multi-air conditioner using electronic expansion valves. Energy 28, 141-155.
4. Dobson, M.K. and Chato, J.C., 1998. Condensation in smooth horizontal tubes. ASME Journal of Heat Transfer 120, 193-213.
5. Elliott, M.S. and Rasmussen, B.P., 2013. Decentralized model predictive control of a multiple evaporator air conditioning system. Control Engineering Practice 21, 1665-1677.
6. Gnielinski, V., 1976. New equations for heat and mass transfer in turbulent pipe and channel flow. Int. Chem. Eng. 16 (2), 359-368.
7. Gungor, K.E. and Winterton, R.H.S., 1987. Simplified general correlation for saturated flow boiling and comparisons of correlations with data. Chem. Eng. Res. Des. 65, 148-156.
8. Lemmon, E.W., Huber, M.L., McLinden, M.O., 2010. NIST reference fluid thermodynamic and transport properties - REFPROP version 9.0, National Institute of Standard and Technology.
9. Li, B. and Alleyne, A., 2010. A Dynamic Model of a Vapor Compression Cycle with Shut-down and Start-up Operations. International Journal of Refrigeration 33, 538-552.
10. Park, Y.C., Kim, Y.C., Min, M.K., 2001. Performance analysis on a multi-type inverter air conditioner. Energy Conversion and Management 42 (13), 1607-1621.
11. Shah, R., Alleyne, A.G., Bullard, C.W., 2004. Dynamic modeling and control of multi evaporator air conditioning systems. ASHRAE Trans. 110 (Part 1), 109-119.
12. Shao, S., Xu, H., Tian, C., 2012. Dynamic simulation of multi-unit air conditioners based on two-phase fluid network model. Applied Thermal Engineering 40, 378-388.
13. Wang, C.C., Lee, C.J., Chang, C.T., Lin, S.P., 1999. Heat transfer and friction correlation for compact louvered fin-and-tube heat exchangers. Int. J. Heat Mass Transfer 42, 1945-1956.
14. Wang, C.C., Lin, Y.T., Lee, C.J., 2000. Heat and momentum transfer for compact louvered fin-and-tube heat exchangers in wet conditions. Int. J. Heat Mass Transfer 43, 3443-3452.
15. Winkler, J., 2009. Development of a component based simulation tool for the steady state and transient analysis of vapor compression systems. Ph.D. thesis, University of Maryland College Park.
16. Xu, X., Yan, P., Deng, S., Xia, L., Chan, M., 2013. Experimental study of a novel capacity control algorithm for a multi-evaporator air conditioning system. Appl. Therm. Eng. 50, 975-984.
17. Zhang, W.J. and Zhang, C.L., 2011. Transient modeling of an air conditioner with a rapid cycling compressor and multi-indoor units. Energy Conversion and Management 52 (1), 1-7.
18. Zhou, Y.P., Wu, J.Y., Wang, R.Z., Shiochi, S., Li, Y.M., 2008. Simulation and experimental validation of the variable-refrigerant-volume (VRV) air-conditioning system in EnergyPlus. Energy and Buildings 40, 1041-1047.
19. Zhu, Y., Jin, X., Du, Z., Fan, B., Su, S., 2013. Generic simulation model of multi-evaporator variable refrigerant flow air conditioning system for control analysis. Int. J. Refrigeration 36, 1602-1615.
20. Zivi, S.M., 1964. Estimation of steady-state steam void-fraction by means of the principle of minimum entropy production. ASME Trans. J. Heat Transfer 86, 247-252.